Received: 31 July 2023 | Revised: 10 September 2023 | Accepted: 18 September 2023

DOI: 10.1002/pc.27806

RESEARCH ARTICLE

Polymer COMPOSITES WILEY

Material properties of spray-dried cellulose nanocrystal reinforced homopolymer polypropylene composites

Xueqi Wang[1] | Pixiang Wang[2] | Shaoyang Liu[2] | Justin Crouse[3] | Douglas J. Gardner[3,4] | Brian Via[1] | Tom Gallagher[1] | Thomas Elder[5] | Yucheng Peng[1]

[1]College of Forestry, Wildlife, and Environment, Auburn University, Auburn, Alabama, USA

[2]Department of Chemistry and Physics, Troy University, Troy, Alabama, USA

[3]School of Forest Resource, University of Maine, Orono, Maine, USA

[4]Advanced Structures and Composites Center, University of Maine, Orono, Maine, USA

[5]USDA-Forest Service Southern Research Station, Auburn, Alabama, USA

Correspondence
Yucheng Peng, College of Forestry, Wildlife, and Environment, Auburn University, 520 Devall Drive, Auburn, AL 36849, USA.
Email: yzp0027@auburn.edu

Funding information
Alabama Agricultural Experiment Station; Hatch program of the USDA National Institute of Food and Agriculture, Grant/Award Number: ALA031-1-19091; Southern Research Station; U.S. Endowment for Forestry and Communities

Abstract

Spray-dried cellulose nanocrystal (SDCNC) particles have attracted intense interest as reinforcements in polymer composites because of their unique physical and mechanical properties. This work aims to develop homopolymer polypropylene (HPP) composites with different loading levels of SDCNC particles (5, 10, 15, and 30 wt%) to understand their impact on composite mechanical, morphological, and thermal properties. The SDCNC-reinforced HPP composites were manufactured using a C.W. Brabender bowl internal mixer with a masterbatch concept and an injection molding process. The mechanical, morphological, and thermal properties of the composites were investigated. Compared to pure HPP, the tensile, and flexural modulus of elasticity (MOE) of composites with 30 wt% SDCNC significantly increased by up to 67% and 49%. The impact strength of the composites with the absence of a compatibilizer significantly increased by up to 19%, which was attributed to the mechanical interlocking network established between SDCNC particles and HPP. Additionally, increasing SDCNC loading in the composites led to higher crystallization peak temperatures and increased the degree of crystallinity (especially at 30 wt% SDCNC content), indicating that the SDCNC particles can act as heterogeneous nucleating agents during the crystallization process. The thermal stability of the composite was slightly improved upon SDCNC introduction.

Highlights

- With the incorporation of spray-dried cellulose nanocrystal (SDCNC), the tensile modulus of elasticity (MOE), flexural MOE, and impact strength of filled homopolymer polypropylene (HPP) composites were significantly improved by up to 67%, 49%, and 19%, respectively.
- Mechanical interlocking network established between SDCNC and HPP contributed to the enhanced the impact strength.
- SDCNC particles can act as heterogeneous nucleating agents to promote the crystallization process of HPP.
- SDCNC particles slightly enhanced the thermal stability of HPP composite.

KEYWORDS

mechanical interlocking, mechanical properties, morphology, nucleation agent, spray-dried cellulose nanocrystals, thermal stability

1 | INTRODUCTION

Cellulose nanocrystals (CNCs), a type of nanomaterial extracted from lignocellulosic-based feedstocks, have a rod-like structure with diameters of 5–10 nm and lengths ranging from a few hundred nanometers to a few micrometers.[1] CNCs can be extracted from diverse lignocellulosic biomass sources by different mineral and organic acids hydrolysis methods and TEMPO-mediated oxidation, which determine the unique characteristics of CNCs.[2,3] After acid treatment, most of the amorphous regions of cellulose are removed, resulting in CNCs containing only a small amount of defects with a high degree of crystallinity, which makes CNCs possess remarkable mechanical properties. The modulus of elasticity (MOE) and tensile strength of CNC are about 130 GPa and up to 10 GPa, respectively, which are significantly higher than those of natural fibers, such as kenaf, flax, cotton, and bamboo.[4,5] Additionally, CNCs have the benefits of high surface area, low density, non-toxicity, biodegradability, and renewability compared with synthetic fibers, such as glass fibers.[6] These characteristics of CNCs make it a promising candidate for reinforcing polymer composite materials.

Thermoplastic polymer composites reinforced by CNCs have attracted tremendous attention and improvements in the properties of many polar and nonpolar polymer matrices have been realized.[7–12] Polypropylene (PP) is the most widely used thermoplastic for commodity materials because of its favorable characteristics, including light weight, flexible processing techniques, and recyclability.[13,14] Compared to other commodity plastics, such as polyethylene, the higher melting point, chemical resistance, stiffness and rigidity, and heat resistance of PP make it a popular choice as a matrix.[15] It was observed that adding CNCs to PP enhanced the mechanical and thermal properties when different process methods were used.[9,16–18] Bahar et al[18] successfully prepared PP composites reinforced by CNCs at concentrations ranging from 5 to 15 wt% via a solution casting process. They found that the tensile strength and Young's modulus of filled PP composites increased by about 81% and 19%, respectively. Sojoudiasli et al[16] developed CNCs-reinforced PP composites by the melt compounding technique and observed that when compared with neat PP, tensile modulus of elasticity and strength of the composites with 2 wt% CNCs was improved by about 30% and 16%, respectively. Both the solution casting and melt compounding methods are successful for developing composites with desirable performance. However, in order to meet the large-scale manufacturing that needs a cost- and energy-effective process, this study used the melt compounding approach because it is solvent-free and more flexible than solution casting when manufacturing nonpolar polymer matrix composites.

In practice, drying CNCs is a pre-requisite for melt compounding with polymers because CNCs are commonly obtained in the form of an aqueous suspension once other impurities and amorphous cellulose are removed from acid treatment solution. Various drying methods such as oven, freeze, spray, and supercritical drying have been evaluated.[19,20] The spray drying method has been suggested as the most appropriate technique for producing dried CNCs as fillers in composite manufacturing through a melt compounding process because of its simple process, rapidity, efficiency, low cost, and scalablity compared to other drying methods.[2,20–22] Notably, the morphologies of CNCs particles were changed from needle-like to donut-shaped or mushroom cap structures after being subjected to spray drying. Changes in particle size from the nanoscale to the microscale was also demonstrated.[23] It is well-known that nanosized CNCs and freeze-dried CNCs exhibit great reinforcing ability in polymer composites.[24–26] The potential capability of spray-dried CNCs (SDCNCs) in improving the mechanical properties of polymer composites deserves to be explored.

CNCs can also be a promising toughening agent to improve polymer composite impact resistance that is one of the important mechanical characteristics determining the ability of a material to withstand fracture or failure under a load or impact.[8,12,13,27] This reinforcibility of CNCs particles can promote to address the issue that the application of PP in structural applications where impact resistance is critical, such as in construction materials, automotive parts, or sporting equipment, is limited because of the low impact resistance of PP. A study reported that SDCNC particles increased the impact strength of PP composite from 21.96 to 24.2 J m^{-1} without any compatibilizer in the system.[28] However, the literature by Agarwal et al[28] did not provide a clear explanation regarding the enhancement mechanism in impact resistance after incorporating SDCNC particles with the PP matrix, and did not study the effect of SDCNC particles at different loading levels on this

performance. Herein, this work will pay close attention to the potential mechanism of the effect of SDCNC particles on the impact strength of PP composites. Simultaneously, the influence of CNCs in suspension format and dry format (freeze-, oven-, and spray freeze-dried CNCs) on crystallization behavior of polymer composites has been extensively studied, indicating that CNCs can act as a nucleating agent in polymer composites, forming a transcrystalline layer around CNCs.[29–34] This research will investigate the effect of SDCNC particles on PP composites' crystallization behavior, which plays a significant role in determining the physical and mechanical behaviors of polymeric composites. In summary, it is essential to figure out the potential reinforcing ability of SDCNC particles in PP composite. Comprehending the fundamental mechanism of the enhanced impact strength is vital for guiding to design and develop materials with tailored properties, expanding the opportunities of PP composites with improved properties.

The current work aims to understand the reinforcing effect of the irregularly shaped SDCNC particles with micrometer sizes on the behavior of PP composites. A melt compounding process was used to manufacture SDCNC-reinforced homopolymer polypropylene (HPP) composites with a masterbatch concept, which is an effective approach to achieve good dispersion of reinforcement in a polymer matrix. Meanwhile, the influence of SDCNC particles at different loading levels ranging from 5 to 30 wt% on the composite properties was also examined. The research results indicated that SDCNC particles had a remarkable capability to improve the mechanical properties of PP composite with the absence of any compatibilizer. A possible mechanism explaining this enhancement was proposed. The thermal behaviors of SDCNC-reinforced PP composites were also discussed regarding crystallization characteristics and thermostability.

2 | MATERIALS AND METHODS

2.1 | Materials

A commercial grade HPP with a density of 0.9 g cm^{-3} used as the matrix in this study was provided by ExxonMobil Chemical Company (ExxonMobil™ PP1264E1, Houston, TX). The SDCNCs in the form of powder was supplied by CelluForce (Montreal, Canada). As reported by the supplier, the bulk density of SDCNC powder is 0.7 g cm^{-3}, and the crystalline fraction and specific surface area are 0.88 (by XRD) and 400 m^2 g^{-1}, respectively. In addition, the CNC powder has a sulfur content of 0.86–0.89 wt%. The SDCNC powder was stored in a sealed container in the freezer before use.

2.2 | SDCNC characterization

The particle size distribution of the SDCNCs was determined according to the process published in previous work.[35] The analysis was performed using a Mastersizer 2000 particle size analyzer (Malvern Instruments, Malvern, UK) with the Sirocco 2000 dry dispersion unit. The measurement was conducted at four-bar air pressure and 20% feeder capacity. Three replicates were measured. The morphologies of SDCNC particles were examined using a Zeiss Evo 50VP scanning electron microscope (Oberkochen, Germany) operated at an accelerating voltage of 20 kV. The SDCNC particles were uniformly deposited on a conductive carbon tape, followed by sputter coating with gold for 60 s using a Q150R ES sputter coater (Hatfield, PA, USA) prior to the Scanning electron microscopy (SEM) characterization.

2.3 | Preparation of HPP/SDCNC composites

The HPP/SDCNC composites were prepared using a concept of masterbatch, which is an effective method to help the uniform dispersion of particles into polymer matrix.[35–37] The masterbatch with a high concentration of SDCNC particles (30 wt% based on the weight of composites, the sum of the weights of SDCNC and HPP) was prepared in the first step. Then the masterbatch was diluted by adding fresh HPP pellets to reach the designed loading level of SDCNC. The resultant filled HPP composites are denoted as 5CNC, 10CNC, 15CNC, and 30CNC, representing the composites containing 5, 10, 15, and 30 wt% SDCNC particles in HPP composite, respectively.

All masterbatch and final composites were prepared using a C.W. Brabender bowl mixer (CWB-2128, Hackensack, NJ, USA) with a maximum capacity of 200 g operated at 200°C with the two roller blades rotating counterclockwise at 60 RPM. For masterbatch composites manufacturing, the SDCNC particles were oven dried at 105°C overnight to eliminate the potential moisture before melt compounding. HPP pellets were melted initially for 5 min in the mixer chamber. The SDCNC particles were then added slowly to the mixer. The mixture of SDCNC and HPP was then continued for another 5 min to obtain well-dispersed composites with stabilized mixing torque measured from the internal batch mixer. The composites were then removed from the mixer and solidified, followed by grinding into a pellet format using a low-speed granulator (Shini Plastic Technologies, Inc., Willoughby, OH, USA) with a sieve size of 3 mm. For the final composite manufacturing, the masterbatch pellets were dry blended with fresh HPP pellets before feeding to the internal mixer.

The blended mixture was then mixed for 5 min. All composites containing SDCNC particles were dried overnight in an oven before each thermal processing at 105°C. Pure HPP was manufactured using the same melt compounding procedure as the control sample.

The final composite pellets from each formulation were dried at 105°C overnight and then injection molded (Proto-Ject 150HP, Manning Innovations, Inc., Halls, TN, USA) into standard specimens with specific dimensions for tensile, impact, and flexure tests according to the ASTM standards D638 (Type IV), D256, D790, respectively. The injection molding machine was operated at barrel and nozzle temperatures of 200°C. The impact and flexural samples were injection molded at 44 MPa and the tensile samples were injection molded at 53 MPa. The samples were kept in the mold for 10 s to pack during the injection molding process. The injection molded samples were then put into Ziploc bags and stored in desiccators at room temperature for at least 48 h to avoid absorbing moisture before testing.

2.4 | Composite mechanical property measurements

All mechanical property measurements were performed at 23 ± 2°C with a relative humidity of 50% ± 5%. Tensile tests were conducted according to ASTM D638 (Type IV) using a Mark-10 ESM750s motorized test machine (Copiague, NY, USA) with a 2500-N load cell. An Epsilon extensometer SN E109112 (Jackson, WY, USA) was used to determine the strain of the test composites as the samples were stretched. The testing speed and nominal strain rate at the start of the test were 5 mm min^{-1} and 0.1 mm (mm $min)^{-1}$. Tensile strength (stress at yield point), tensile strain (percentage elongation at yield), and tensile MOE were calculated from seven replicates and reported for neat HPP and all HPP/SDCNC composites. Flexural tests (3-point bending tests) were carried out according to ASTM D790-A using a Mark-10 ESM750s motorized test machine (Copiague, NY, USA) attached with a 500-N load cell. A support span length of 50 mm was employed. The speed of crosshead motion was 1.34 mm min^{-1} for all specimens. Five replicates were tested for each sample. Flexural strength and MOE for all samples were reported. The impact strength of all samples was evaluated according to ASTM D256 using an XJUD Digital Charpy Izod Impact Testing Machine (Deli Group Co. Ltd., Ningbo, China). All specimens were notched by a manual Instron CEAST notcher (Norwood, MA, USA) prior to impact tests according to the ASTM D256. Ten replicates were tested to calculate the average values of impact strengths in kg m^{-2} for all samples.

The mechanical properties, including tensile, flexural, and impact properties, were statistically analyzed with a 0.05 significance level using one-way ANOVA process. The fracture surfaces of impact-tested specimens were sputter-coated for examination using a Zeiss Evo 50VP scanning electron microscope (Oberkochen, Germany) operated at an accelerating voltage of 20 kV. Sputter coating was performed using a Q150R ES sputter coater (Hatfield, PA, USA) with gold for 60 s.

2.5 | Water absorption tests

Water absorption tests were conducted using the impact fractured specimens to study the water resistance of the composites. The measurements were performed according to ASTM D570. Initially, all specimens were dried at 105°C in an oven to a constant weight. The initial sample weight and dimensions (thickness and width) were recorded to the nearest 0.0001 g using an electronic weighing balance (VWR-64B2, VWR, USA) and to the nearest of 0.001 mm using a digital micrometer (293-340-30, Mitutoyo, Japan). The thickness and width measurements were averaged from at least three points for each sample. The specimens were then immersed in containers filled with deionized water maintained at a room temperature of 23 ± 2°C. The specimens were removed from the container daily for the first week, and then at 1 or 2-week intervals, and extra water on the sample surface was wiped with tissue paper. The sample weight and dimensions were then immediately recorded. After each measurement, the specimens were immersed in the same containers. Five specimens were tested for each sample. The percentages of water gain, thickness swell, and width swell were calculated using the following equations:

$$\text{Water gain}\,(\%) = \frac{W_t - W_0}{W_0} \times 100 \quad (1)$$

$$\text{Thickness swell}\,(\%) = \frac{T_t - T_0}{T_0} \times 100 \quad (2)$$

$$\text{Width swell}\,(\%) = \frac{w_t - w_0}{w_0} \times 100 \quad (3)$$

where W_0, T_0, and w_0 are the initial weight, thickness, and width of the specimens after oven-dried, W_t, T_t, and w_t are the weight, thickness, and width of specimens after immersion for different times, respectively.

2.6 | Thermal properties

The crystallization and melting behaviors of all the composites were investigated using a DSC-250 differential

scanning calorimeter (TA Instruments, DE, USA) under an N_2 atmosphere with a flow rate of 50 mL min^{-1}. Samples of about 10–15 mg were sealed in a Tzero pan. The DSC measurement was carried out by heating the specimen from 40 to 200°C, then maintaining it at 200°C for 2 min to remove any previous thermal history. The specimen was then cooled to 40°C at 10°C min^{-1} to investigate their crystallization behaviors. Finally, the melting behaviors were characterized by reheating the specimen to 200°C at 10°C min^{-1}. Each sample was measured in triplicate. The TRIOS (TA Instruments, DE, USA) software was used to analyze all the data. The degree of crystallinity X_c (%) was calculated by the following equation:

$$X_c\,(\%) = \frac{\Delta H_m}{\Delta H_m^0\, w_{HPP}} \times 100\% \quad (4)$$

where ΔH_m is the measured melting enthalpy, ΔH_m^0 is the melting enthalpy of 100% HPP (205 J mol^{-1}),[38] and w_{HPP} is the weight fraction of HPP in the composite.

The thermostability of all the samples was characterized by thermogravimetric analysis (TGA) using a TGA-550 analyzer (TA Instruments, DE, USA). The measurement was carried out under nitrogen with flow rates of 60 and 40 mL min^{-1} for sample and balance purge, respectively. All samples (8–16 mg) were heated from 40 to 600°C with a heating rate of 10°C min^{-1}. Three replicates were tested for each sample. The TRIOS (TA Instruments, DE, USA) software was used to analyze the TGA and DTG (derivative thermogravimetric curve that is a plot of the rate of mass change with respect to temperature) curves.

2.7 | Melt flow index

The melt flow index (MFI) measurements of pure HPP and HPP/SDCNC composites were performed using an MFI testing instrument (Techtongda, Markham, ON, Canada) in accordance with ASTM D1238. The pellet samples of about 7 g obtained from the granulator were compacted and preheated for 4 min in the barrel. The MFI measurement was carried out at 200°C with a constant load of 2.16 kg to keep SDCNC from thermal degradation during the measurement. Six replicates were collected and weighed for each sample.

3 | RESULTS AND DISCUSSION

3.1 | The SDCNC particle characteristics

The volume-based particle size distribution of the SDCNC particles is shown in Figure 1A and a single peak with particle sizes ranging from 0.90 to 90 μm was obtained. The results indicated that the particle size at 10, 50, and 90 percentiles was 5.54 ± 0.14, 17.83 ± 0.13, and 38.72 ± 0.17 μm, that is, 50% of the particles have a size smaller than 17.83 μm. The morphologies of SDCNC particles were characterized by SEM at different magnifications. The SDCNC particles possess irregular shapes with a broad range of sizes, as shown in Figure 1B. Some SDCNC particles are twisted or folded, forming large dense agglomerates with sizes of up to 40 μm. The SDCNC particles exhibit a mushroom cap or donut shape, similar to previous results.[23] The wrinkled profiles and cracks on the surface of SDCNC particles are also observed from the micrographs at high magnifications, as identified by the white arrows in Figure 1C–E. The irregular features of SDCNC particles are attributed to the influence of three fundamental forces, including hydrogen bonding, van der Waals forces, and capillary forces, experienced during the spray drying process.[19] These forces are responsible for governing individual CNC particles together, adhering to each other, and influencing the overall structure of dried particles.

3.2 | Mechanical properties of the composites

The mechanical performance of all composites was characterized, including tensile, flexural, and impact properties, according to the ASTM D638, D790, and D256, respectively. The statistical analysis results of all the composites' mechanical properties are summarized in Table 1.

The tensile properties were measured to determine the influence of different loadings of SDCNC particles on tensile MOE, strength, and strain. The properties of pure HPP and HPP/SDCNC composites are summarized in Table 1. The appearance of neat HPP was translucent, while the color of the composites became browner with the incremental loading levels of SDCNC in the composites. The color change may be ascribed to the presence of sulfate groups of the SDCNC particles in the composites, which are susceptible to thermal degradation at high temperatures in the thermal compounding and injection molding processes.[39] All the composites exhibit the same tendency under the tensile load, and the representative tensile stress–strain curves were recorded from the starting point to the yield point in the tensile test, as represented in Figure 2. Elastic deformation occurs initially within a small strain range with the highest deformation rate. The MOE is calculated based on the slope of this linear section of the stress–strain curve (zoom-in portion of the curve). Then, the stress–strain curve follows a

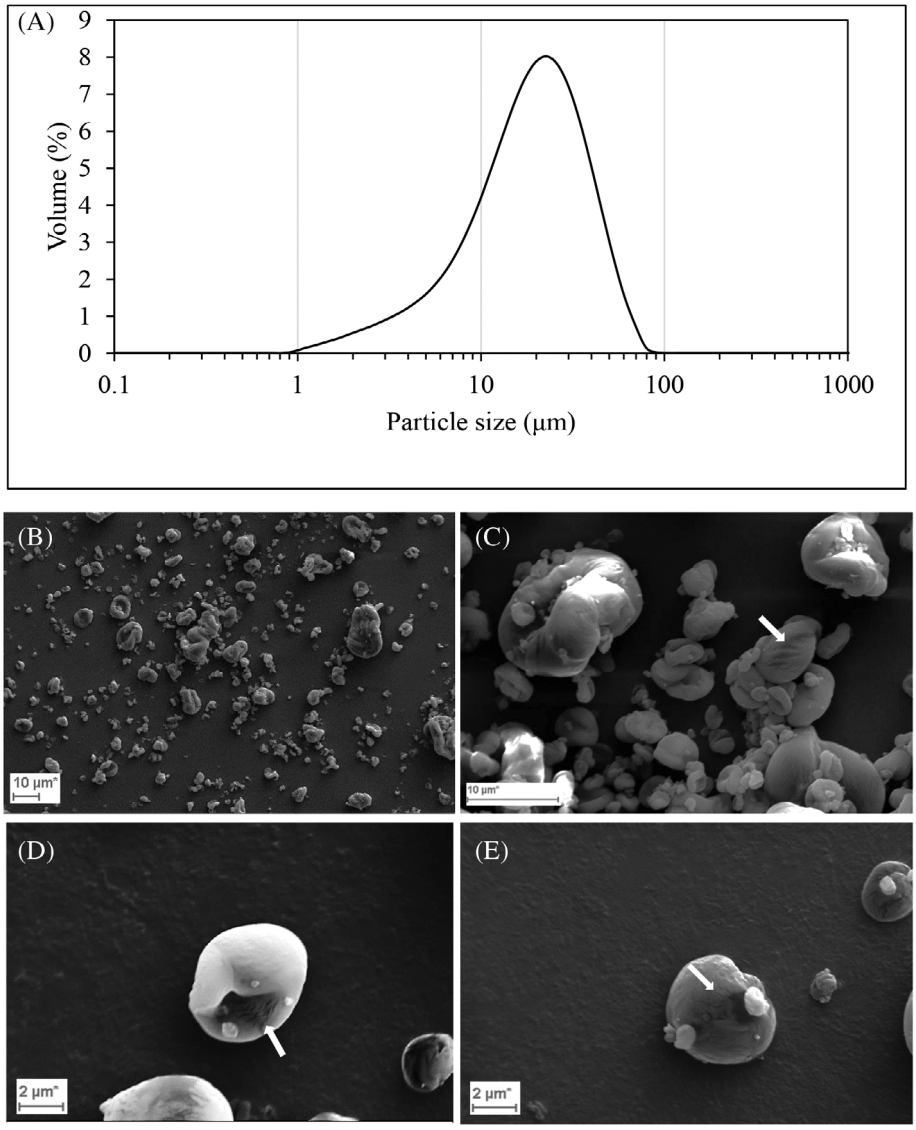

FIGURE 1 The particle size distribution of spray-dried cellulose nanocrystal (SDCNC) particles (A) and the morphologies of SDCNC particles (B–E, B: ×1000; C: ×5000; D and E: ×8000).

TABLE 1 The mechanical properties of SDCNC particles reinforced HPP composites.

	Tensile properties			Flexural properties		Impact strength	Melt flow index
Sample	MOE (GPa)	Strength (MPa)	Strain (%)	MOE (GPa)	Strength[c] (MPa)	(kJ m^{-2})	(g [10 min]$^{-1}$)
HPP	1.34 ± 0.03[a] D[b]	30.2 ± 0.2 A	10.3 ± 0.6 A	1.32 ± 0.02 D	40.7 ± 0.5 C	1.62 ± 0.12 B	7.04 ± 0.07 A
5CNC	1.66 ± 0.02 C	30.4 ± 0.4 A	8.5 ± 0.3 B	1.32 ± 0.02 D	39.5 ± 0.4 D	1.78 ± 0.19 AB	6.77 ± 0.07 B
10CNC	1.76 ± 0.05 B	29.1 ± 0.2 B	7.5 ± 0.4 C	1.50 ± 0.02 C	42.8 ± 0.7 B	1.91 ± 0.12 A	6.19 ± 0.08 C
15CNC	1.86 ± 0.02 B	26.9 ± 0.3 C	7.1 ± 0.3 C	1.66 ± 0.07 B	44.2 ± 0.7 A	1.92 ± 0.13 A	6.22 ± 0.10 C
30CNC	2.24 ± 0.16 A	22.0 ± 0.7 D	4.0 ± 0.2 D	1.96 ± 0.02 A	41.3 ± 0.2[d] C	1.85 ± 0.14 A	4.98 ± 0.10 D

Abbreviations: HPP, homopolymer polypropylene; MOE, modulus of elasticity; SDCNC, spray-dried cellulose nanocrystal.
[a]Data were statistically analyzed by the average ± standard deviation.
[b]Values within a column with different letters, A, B, C, D, and E, indicate the significant difference at $p \leq 0.05$ between the samples. One way ANOVA followed with Tukey post hoc process was used to statistically analyze all data.
[c]Flexural strength is reported by the stress at 5% strain since neither break nor yield occurred for pure HPP, 5CNC, 10CNC, 15CNC composite samples.
[d]Flexural strength of 30CNC composite is reported by the stress at the yield point.

viscoelastic deformation, where the deformation rate decreases, and the stress reaches a maximum value at the yield point.

The tensile strength of pure HPP is 30.2 ± 0.2 MPa, and the composite of 5CNC maintains the tensile strength at a similar level (30.4 ± 0.4 MPa). However, a

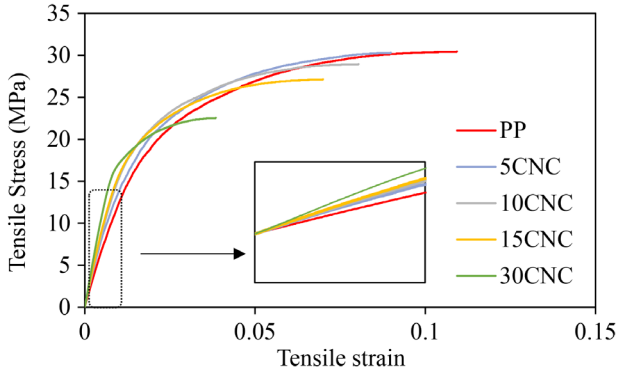

FIGURE 2 The representative tensile stress–strain curves of all the composites.

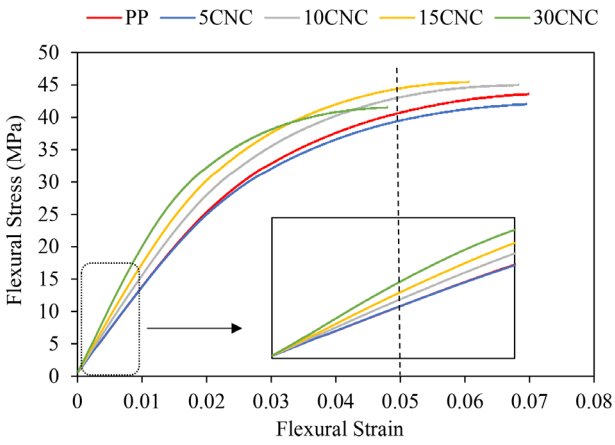

FIGURE 3 The representative flexural stress–strain curves of all the composites.

significant reduction in tensile strength of HPP/SDCNC composites at higher SDCNC loadings is observed (Table 1), although SDCNC particles possess a higher theoretical tensile strength (7.5–7.7 GPa) than HPP.[5] The tensile strength decreased to 29.1 ± 0.2, 26.9 ± 0.3, and 22 ± 0.7 MPa for the 10CNC, 15CNC, and 30CNC composites, which were 4%, 11%, and 27% lower than that of neat HPP, respectively. This reduction is possibly attributable to the inherent incompatibility between hydrophilic SDCNC and hydrophobic HPP and the remarkably different surface energies of SDCNC (60.7 mJ m^{-2}) and HPP (around 30 mJ m^{-2}).[40,41] The incompatibility and varying surface energies result in the weak or no interfacial bonding between the two phases and the separated interface (as shown in the Figure 4, discussed in the following impact results section), which further lead to a lower stress transfer efficiency from the HPP matrix to the SDCNC particles under the applied tensile force.

On the other hand, the tensile MOE of HPP/SDCNC composites progressively increases with increasing the SDCNC content (Table 1). The values of tensile MOE increased from 1.34 ± 0.03 GPa (HPP) to 1.66 ± 0.02, 1.76 ± 0.05, 1.86 ± 0.02, and 2.24 ± 0.16 GPa for the composites of 5CNC, 10CNC, 15CNC, and 30CNC, which are approximately 23%, 31%, 38%, and 67% higher than that of pure HPP. The increase of MOE is caused by the higher stiffness of SDCNC (around 100–130 GPa) embedded in a lower MOE HPP matrix.[42] Incorporating SDCNC particles at high loadings in composites can decrease the plastic deformability of a polymer matrix while increasing the elastic response.[19]

Meanwhile, the tensile strain at yield gradually decreased from 10.3% ± 0.6% (HPP) to 8.5% ± 0.3%, 7.5% ± 0.4%, 7.1% ± 0.3%, and 4.0% ± 0.2% for filled composites, which decreased by 18%, 27%, 31%, and 62% relative to pure HPP (Table 1). This indicated a reduced ductility or more brittleness of HPP/SDCNC composites compared with neat HPP. The decrease of strain at yield for composites containing SDCNC can be explained not only by the poor interfacial adhesion between SDCNC and the HPP matrix in the absence of compatibilizer (Figure 4), but also by the decreased polymer molecular chain movement restricted by the SDCNC particles under the tensile load.

The flexural properties, including flexural strength and MOE, of the pure HPP and HPP/SDCNC composites are shown in Table 1. The representative flexural stress–strain curves are shown in Figure 3. Flexural strength is determined as the stress at the yield point for 30CNC and the stresses at 5% strain for pure HPP, 5CNC, 10CNC, and 15CNC composites since these composites did not yield or break within the 5% strain limit (Figure 3). The flexural MOE and strength of pure HPP are 1.32 ± 0.02 GPa and 40.7 ± 0.5 MPa, respectively. With the addition of SDCNC particles into HPP, a similar trend to tensile MOE was observed for flexural MOE. Adding SDCNC particles in the HPP matrix significantly increased the flexural MOE because of the addition of SDCNC particles with a higher stiffness in HPP composites (Table 1). The values of flexural MOE for composites 10CNC, 15CNC, and 30CNC are 1.50 ± 0.02, 1.66 ± 0.07, and 1.96 ± 0.02 GPa, representing an increase of 14%, 26%, and 49% when compared to the neat HPP. The highest flexural strength is observed in the case of the 15CNC composite (44.2 ± 0.7 MPa), which is an enhancement of 8% as compared to pure HPP. There is no significant difference in flexural strength for 30CNC compared to HPP. The composites undergo a complex deformation during the flexural test, including the compression on the top surface and the tension on the bottom surface of composites. Higher stress is needed to reach 5% strain on the bottom surface for 10CNC and 15CNC than that required in pure HPP, thus increasing the flexural strength.[43]

The impact property determines the material deformation behavior when subjected to a high deformation

rate. The results of notched Izod impact tests for all the composites are given in Table 1. The HPP/SDCNC composites demonstrate an improvement in impact resistance. The impact strength is 1.62 ± 0.12 kJ m^{-2} for pure HPP, and the values are 1.78 ± 0.19, 1.91 ± 0.12, 1.92 ± 0.13, and 1.85 ± 0.14 kJ m^{-1} for 5CNC, 10CNC, 15CNC, and 30CNC composite, representing 10%, 19%, 19%, and 15% enhancements as compared to pure HPP, respectively. The composite of 30CNC has a slightly lower value, but the number is still significantly higher than that of pure HPP. Adding SDCNC particles in HPP significantly improves the impact strength of HPP/SDCNC composites based on the statistical analysis compared to pure HPP. There is no significant change between composites with different content of SDCNC particles. This remarkable enhancement indicates that the SDCNC particles can absorb the impact energy when subjected to a high strain rate.[8] The morphologies of impact fractured surface of all HPP/SDCNC composites were investigated by SEM (Figure 4). Pure HPP behaves the typical homogenous polymer fractured surface, and the surface becomes rougher after adding rigid SDCNC particles, as shown in Figure 4A–C. The coarser fracture surfaces indicate that more interfacial surface areas between SDCNC particles and HPP matrix were created by increasing the SDCNC loadings. Therefore, the composites can absorb more energy used for separating the interface. As a result, the impact strengths of all HPP/SDCNC composites are higher than that of pure HPP. Meanwhile, the relatively uniform distribution of SDCNC particles at low concentrate in the HPP matrix can be observed (Figure 4B,D,E). The SDCNC particle size after processing is closer to the initial size (around 15 μm), no obvious larger agglomerates are formed. On the fracture surfaces of HPP/SDCNC composites, some SDCNC particles are embedded in the HPP matrix, while some SDCNC particles are pulled out from the matrix. The voids and the interfacial separation can be observed clearly (the white arrow in Figure 4D–F), mainly caused by the inherent incompatibility between hydrophilic SDCNC particles and hydrophobic HPP matrix.

Simultaneously, it is worth noting that from the red circles shown in Figure 4D–F, some stretched polymer filaments are strongly attached to the SDCNC surface after impact tests. This phenomenon can be explained by

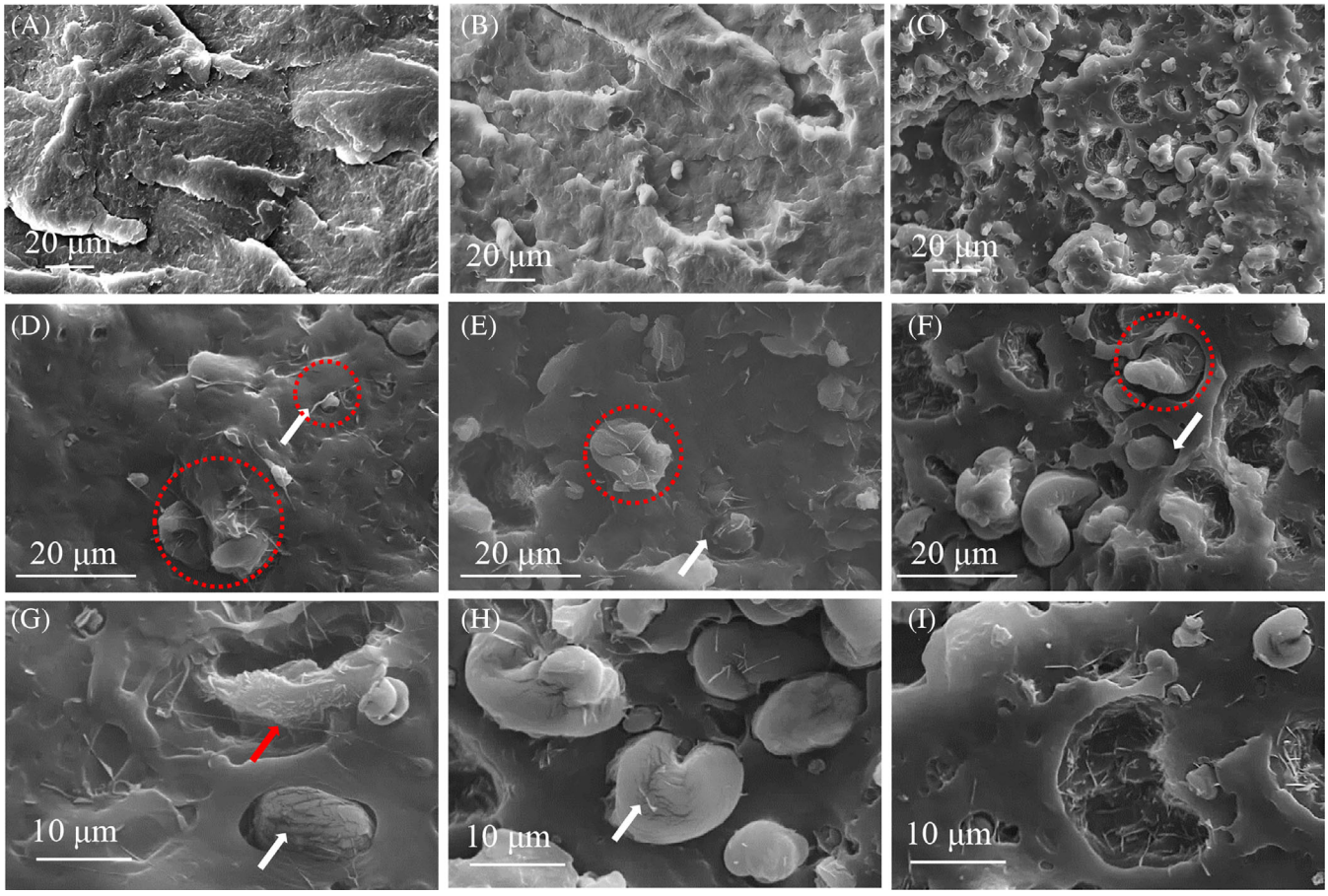

FIGURE 4 The SEM micrographs of fracture surfaces for pure homopolymer polypropylene (A), 5CNC (B), 10CNC (D), 15CNC (E), 30CNC (C–F) and the mechanical interlocking networks between spray-dried cellulose nanocrystal and polymer matrix (G–I). ABC: ×2000, DEF: ×5000, GHI: ×8000.

the theory of mechanical interlocking interfacial adhesion mechanism, where a strong interaction between two or more components was created by the physical interlocking. Polymer matrix can be filled in the holes or cracks on particle or fiber surface, subsequently, the two components can be locked mechanically after curing, enhancing the interfacial adhesion.[44] In this study, the melt HPP can penetrate and be locked into the cracks on the SDCNC during the composite solidification process, increasing the interfacial surface area and physical interaction between SDCNC and HPP and promoting the plastic deformation of the polymer matrix during impact testing. When composites are subjected to a high magnitude impact load with a high strain rate, the polymer phase in composites is stretched quickly and then breaks. The process will absorb more energy in fracturing the sample because of the mechanical interlocking network between the two phases. From the SEM micrographs with high magnification, more cracks can be distinctly observed on the SDCNC surface (the white arrow in Figure 4G,H). A broken SDCNC agglomerate was also observed (the red arrow in Figure 4G), meaning greater energy is needed for the rupture of the HPP/SDCNC composites. Rough fracture surfaces (Figure 4I) are clearly identified after pulling out the embedded SDCNC particles from the matrix after the impact test, which indicates the formation of specific interfacial adhesion between SDCNC particles and HPP and supports the hypothesis that a mechanical interlocking network was established between SDCNC and HPP. In summary, the mechanical interlocking between the SDCNC and HPP has a critical influence on the impact strength, compensating for the negative effect of the incompatibility between SDCNC and HPP. Therefore, a significant improvement in impact strength was achieved for HPP/SDCNC composites even without a compatibilizer in the system. However, for the 30CNC composite, the high SDCNC particle loadings generated much more discontinuous surfaces because of interfacial separation caused by the incompatibility (Figure 4C). More voids were also observed in the 30CNC composites (Figure 4C,F), which results in the lack of effective stress transfer from the HPP matrix to SDCNC particles and accelerates the de-bonding and the deformation. In this case, the impact strength of 30CNC composite is slightly lower than that of 15CNC, but it is still higher than pure HPP because of the mechanical interlocking network between SDCNC and HPP matrix.

3.3 | Water absorption tests

The water absorption properties are important characteristics of composites that determine the potential end-use applications when exposed to environmental conditions. Water absorption in CNC-based composites was studied broadly.[7,45–48] The percentage of water gain against time for all composites is shown in Figure 5A. Similar behavior is observed for all the HPP/SDCNC composites. The water gain rate was rapid at the beginning of the immersion, then approached a plateau with a decreasing rate later. In some cases, especially for the 30CNC sample, it did not reach a plateau. The percentages of the water gain, thickness swell, and width swell for all composites after water immersion for 150 days are reported in Table 2. Each data point represents an average of five specimens.

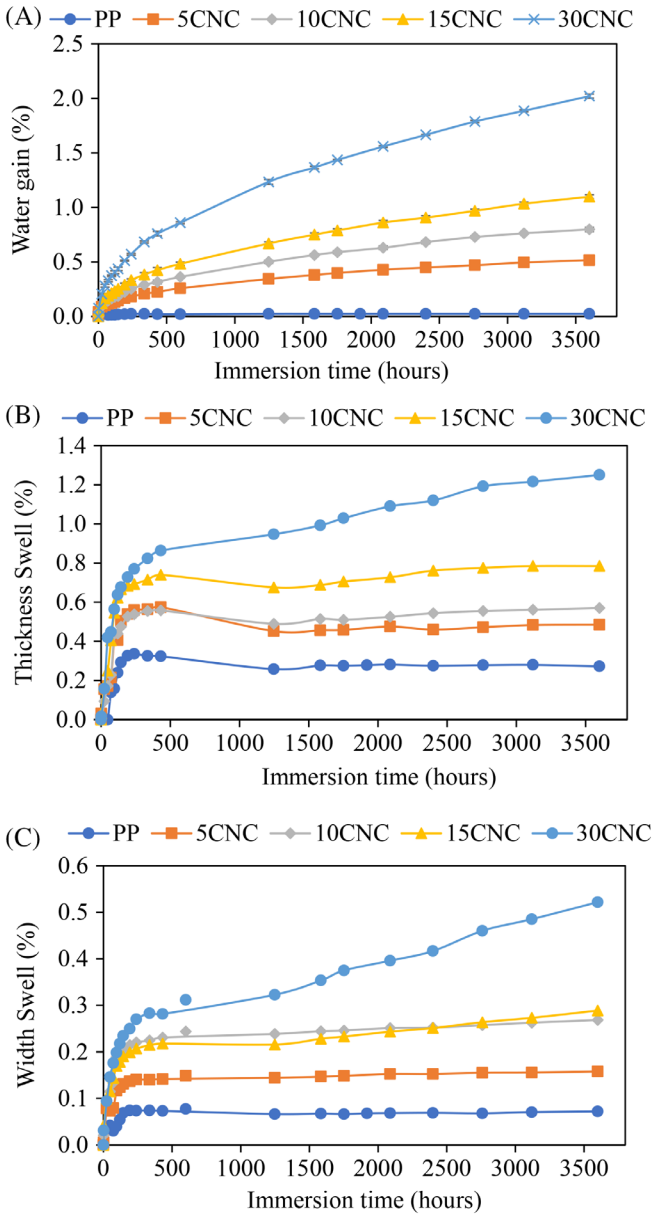

FIGURE 5 The long-term water gain (A), thickness swell (B), and width swell (C) for all composites.

Composite	Water gain (%)	Thickness swell (%)	Width swell (%)
HPP	0.02 ± 0.01	0.27 ± 0.05	0.07 ± 0.05
5CNC	0.52 ± 0.02	0.49 ± 0.16	0.16 ± 0.06
10CNC	0.80 ± 0.02	0.57 ± 0.19	0.27 ± 0.04
15CNC	1.10 ± 0.02	0.79 ± 0.18	0.29 ± 0.08
30CNC	2.02 ± 0.02	1.25 ± 0.25	0.52 ± 0.12

Abbreviations: HPP, homopolymer polypropylene; SDCNC, spray-dried cellulose nanocrystal.

TABLE 2 Water gain and dimensional swelling for pure HPP and HPP/SDCNC composites after immersion for 150 days (3600 h).

Pure HPP absorbs the lowest level of water (0.02%) attributable to the hydrophobic nature of the material. The water gain of the HPP/SDCNC composites continuously increases with the increase in immersion time. Generally, moisture can penetrate into composites by three different mechanisms: (1) water molecules penetrate inside the micro-voids between polymer chains; (2) transportation of water molecules by micro-cracks in the matrix, formed in the compounding process; (3) diffusion into gaps and flaws at the interfaces between polymer and fillers.[49] The water gain of HPP/SDCNC composites is attributable not only to the hydroxyl groups in SDCNC that can attract water molecules through hydrogen bonding promoting water uptake, but also to the poor interfacial compatibility between SDCNC and HPP, generating the gaps in the interface (Figure 4D–F) and accelerating water collection. The amount of water gain depends upon the concentration of SDCNC particles in the composites—higher content of SDCNC particles results in higher water gain since SDCNC particles provide more binding sites for water. However, HPP/SDCNC composites showed little absorption after immersing water for 150 days (around 2%), which was a strong indicator that the most of the SDCNC particles in composites are distributed uniformly encapsulated within the HPP matrix, preventing water molecules from penetrating and contacting the SDCNC particles.

A similar trend was observed for the thickness and width swell Figure 5B,C. The dimensional swell in the thickness direction is higher than that in the width direction. The specimen width (around 12.7 mm) is much higher than the thickness (around 3.2 mm), water molecules have longer diffusion path from surface area to the center of composites along the width direction than in the thickness direction, resulting in the slower rate of diffusion and lower dimension swell in width direction compared to that in thickness direction where diffusion occurred more rapidly. The overall dimensional swelling is low (less than 2%) for all HPP/SDCNC composites. This value is much lower than that of other natural reinforcements in HPP polymer. For example, Ashori et al[50] studied the effect of recycled newspaper fiber and wood flours as reinforcements on moisture absorption and thickness swelling behaviors for PP composites. The results showed that 30 wt% reinforcements significantly influenced the water absorption (12%) and thickness swell (8.5%), which is approximately six times higher than that of HPP/SDCNC composites at the same concentration. In this respect, SDCNC particles as reinforcement in polymer composites behave better than other natural fibers when exposed to a wet environment for a long time.

3.4 | Thermal properties of the composites

The DSC cooling and second heating thermograms of all the composites are shown in Figure 6. The melting and crystallization characteristic parameters, including melting enthalpy (ΔH_m), onset temperature of melting ($T_{on\text{-}m}$), melting peak temperature (T_m), crystallization enthalpy (ΔH_c), onset temperature of crystallization ($T_{on\text{-}c}$), crystallization peak temperature (T_c), and degree of crystallinity (X_c %), are summarized in Table 3. The results clearly show that the addition of different levels of SDCNC to HPP only leads to a marginal influence on the T_m (±1°C) as compared to pure HPP (Figure 6B), and it is not possible to establish a correlation between T_m and the SDCNC loading levels. Similar observations in the case of lignocellulosic material-reinforced HPP composites were reported.[16,51,52] However, it can be seen from Figure 6A that the $T_{on\text{-}c}$ and T_c of the composites gradually increase from 118.0 ± 0.3°C to 127.2 ± 0.1°C and from 112.5 ± 0.1°C to 123.0 ± 0.2°C, respectively, as the SDCNC loading levels increased in HPP, which indicates that the crystallization of HPP started earlier during the cooling process. The temperature increase is probably because of the formation of a transcrystalline layer at the interface between SDCNC and HPP.[31,33,53] Another assumption is that the SDCNC particles within the HPP matrix can act as heterogeneous nucleating agents, allowing for many nucleation sites, promoting the partial crystalline growth of HPP and improving mechanical properties.[51] Meanwhile, as the loading of the SDCNC particles increases, the ΔH_c steadily decreases because a

larger number of rigid particles in HPP restrict the thermal motion of polymer chains and reduce chain mobility for crystallization.[53] There is no significant change in X_c % of HPP after adding SDCNC particles except for the composite of 30CNC. The X_c % of HPP in 30CNC composite increases from 41.3% ± 0.9% (HPP) to 45.0% ± 1.0%. The increase in X_c % contributed to the decrease of the impact strength of 30CNC, which is demonstrated by the results in the mechanical property section.

The thermostabilities of SDCNC and all the composites were investigated by TGA, and the TGA and DTG curves are shown in Figure 7. The TGA curve of the SDCNC can be divided into three sections. The initial weight loss of around 3% occurred at temperatures ranging from 50 to 110°C attributable to the evaporation of moisture from the material.[54] No actual thermal degradation took place in this step. The second major weight loss started at around 292°C, which reached a dominant peak at around 305°C on the DTG curve. This weight loss is attributed to cellulose degradation, including dehydration, depolymerization,

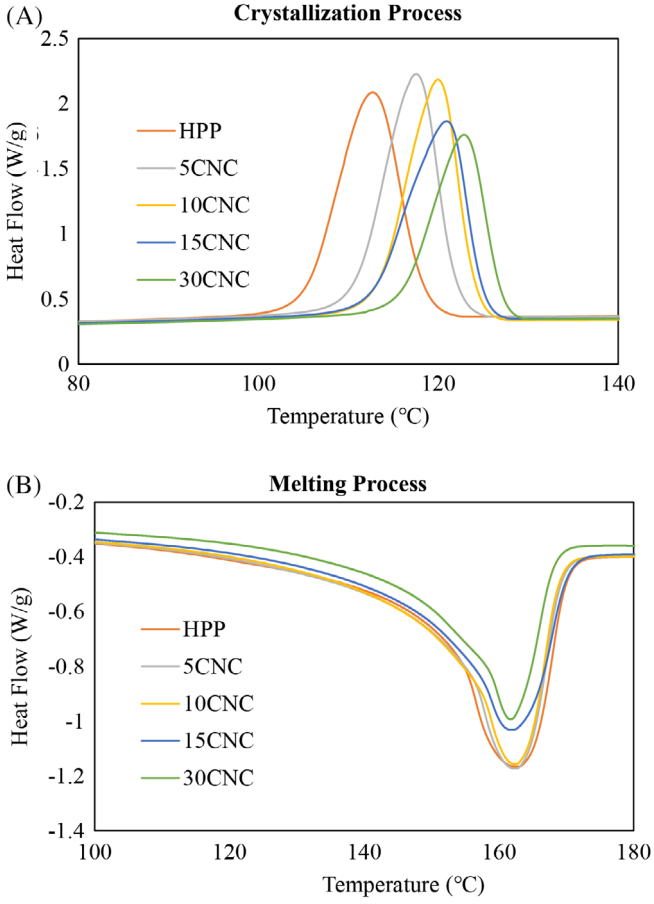

FIGURE 6 The DSC cooling (A) and second heating (B) curves of all the composites.

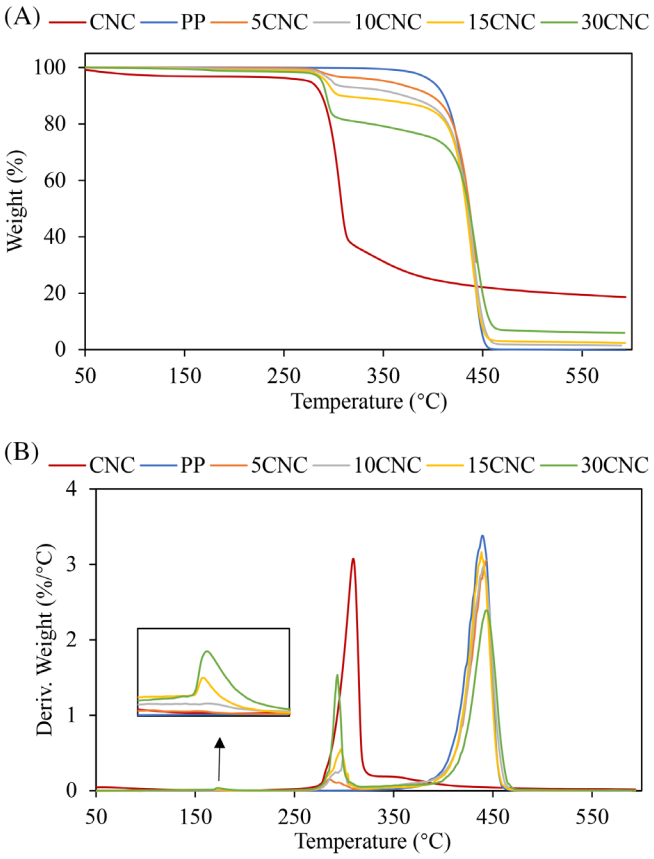

FIGURE 7 The thermogravimetric analysis (A) and Derivative thermogravimetry (DTG) (B) curves for all the samples.

TABLE 3 The melting and crystallization behaviors of all composites.

	Melting process			Crystallization process			
Samples	ΔH_m (J g^{-1})	$T_{on\text{-}m}$ (°C)	T_m (°C)	ΔH_c (J g^{-1})	$T_{on\text{-}c}$ (°C)	T_c (°C)	X_c (%)
HPP	84.7 ± 1.8	151.0 ± 0.3	161.6 ± 0.9	87.0 ± 1.1	118.0 ± 0.3	112.5 ± 0.1	41.3 ± 0.9
5CNC	79.5 ± 3.0	151.3 ± 0.2	162.3 ± 0.3	85.2 ± 1.2	120.8 ± 1.6	116.4 ± 1.7	40.8 ± 1.5
10CNC	76.3 ± 1.1	151.3 ± 0.5	162.5 ± 0.3	80.6 ± 2.4	124.3 ± 0.2	120.3 ± 0.4	41.4 ± 0.6
15CNC	73.9 ± 1.3	152.0 ± 1.8	161.7 ± 0.5	75.3 ± 1.1	125.8 ± 0.7	121.8 ± 0.8	42.4 ± 0.8
30CNC	64.5 ± 1.5	153.6 ± 1.5	161.5 ± 0.1	64.6 ± 0.1	127.2 ± 0.1	123.0 ± 0.2	45.0 ± 1.0

Abbreviation: HPP, homopolymer polypropylene.

decomposition of dehydrocellulose, and char residue formation.[55,56] The third weight loss occurred at around 350°C because of the breakdown of char residues to low-molecular weight products.[56] The residual weight at the end temperature of 600°C for SDCNC is 18.1 ± 0.9 wt%.

For pure HPP and HPP/SDCNC composites, the weight loss is less than 1 wt% at 50–110°C, indicating the trace amount of absorbed moisture in all composites. Based on the TGA and DTG curves, the HPP matrix displays a single-step thermal degradation behavior with an onset temperature of around 417°C and a maximum weight loss rate at around 439°C. The degradation of the HPP/SDCNC composites can be divided into two processes, as reported before, which are ascribed to the degradation of SDCNC (270–300°C) and HPP (420–450°C), respectively.[9,53,57] The other degradation process can be found from the DTG curves at around 150°C for the 15CNC and 30CNC composites, which can be attributed to the presence of sulfate group in SDCNC introduced by the acid hydrolysis process in preparing the CNC material.[58,59] This degradation cannot be identified for 5CNC and 10CNC composites because of the low SDCNC content in the composites. And it is also disappeared for the SDCNC particles from DTG curve. All composites used in the TGA measurements were subjected to the melt compounding process while the SDCNC particles are used in the native form, and the high temperature in the melt compounding process may facilitate the degradation of the SDCNC. This can be explained by the results that the onset temperature of SDCNC decreased from around 292°C to around 280–285°C and the peak temperature at the maximum weight loss rate decreased from around 305°C to around 291–297°C as shown in Table 4. The onset temperature for HPP/SDCNC composites are slightly greater than that of pure HPP indicating the improved thermal stability of HPP composites after introducing the SDCNC particles. This observation is consistent with the literature.[53] The residual weight at the end temperature of 600°C for HPP is negligible, suggesting that HPP has a low thermal stability and char-forming ability.[60] It steadily increased for HPP/SDCNC composites with the increase of SDCNC content, indicating that the SDCNC particles can promote the formation of residual weight of HPP/SDCNC composites.[53]

3.5 | Melt flow index

The MFI data for pure HPP and HPP/SDCNC composites are summarized in Table 1. The MFI of HPP is 7.04 ± 0.07 g/10 min. Adding SDCNC particles into HPP resulted in a lower MFI value, decreasing to 6.77 ± 0.07, 6.19 ± 0.08, 6.22 ± 0.10, and 4.98 ± 0.10 g/10 min for 5CNC, 10CNC, 15CNC, and 30CNC, respectively. Incorporating rigid SDCNC particles into the polymeric matrix hinders the polymeric chain segments' rearrangement and free movement and increases the composite viscosity. This result is similar to other literature in which the MFI value is reduced with increased natural reinforcement content in polymeric material.[61–64]

4 | CONCLUSIONS

In the current work, the effect of the SDCNC particles and their loading levels on the mechanical, morphological, and thermal properties of HPP composites was investigated. The statistical analysis results showed that the mechanical properties of the HPP/SDCNC composites were highly impacted by the SDCNC particle loading level. Incorporating SDCNC particles in HPP composites significantly enhanced the tensile and flexural MOE. The impact strength of the HPP composites was significantly improved by adding SDCNC particles due to the presence of irregular-shaped SDCNC particles through the formation of the mechanical interlocking networks. The low water absorption and dimensional swell of HPP composites indicated that the composites can be properly used in applications where exposure to wet environment factor is a concern. The crystallization peak temperatures of the

TABLE 4 The TGA results for all the composites.

	Region 1		Region 2		Region 3			DTG peak (°C)	
Samples	Onset °C	Weight loss %	Onset °C	Weight loss %	Onset °C	Weight loss %	Residual weight %	SDCNC	HPP
HPP	-	-	-	-	417.27	100.00	0.00	-	439.21
5CNC	-	-	279.46	4.46	421.07	94.90	0.66	291.28	438.77
10CNC	104.63	0.72	287.54	6.89	418.06	91.18	1.46	297.70	437.26
15CNC	116.66	0.85	285.74	8.82	420.73	88.23	2.25	294.48	439.12
30CNC	155.80	1.52	285.13	19.62	424.57	72.84	5.97	292.55	441.56

Abbreviations: HPP, homopolymer polypropylene; TGA, thermogravimetric analysis.

HPP/SDCNC composites increased with increasing SDCNC loading levels, suggesting the SDCNC particles can act as heterogeneous nucleating agents during the crystallization process. A slight improvement in the thermal stability of HPP composites after introducing SDCNC particles was observed. These findings have important implications for expanding the application of SDCNC in thermoplastic composites in specific fields, including packaging, construction, and automotive industries, and providing fundamental information to design and develop the composites with desired performance. However, tensile strength and strain at yield were adversely influenced because of the lack of any compatibilizer to improve the interfacial adhesion between the SDCNC particles and matrix. To address the decreased tensile strength in this study and further improve the mechanical properties of the composites, the further work should enhance the compatibility between the SDCNC particles and HPP matrix by exploring the effect of coupling agents on the composite performance.

AUTHOR CONTRIBUTIONS

Ideas and conceptualization were performed by Xueqi Wang and Yucheng Peng. Material preparation, data collection, and analysis were performed by Xueqi Wang, Yucheng Peng, Pixiang Wang, Shaoyang Liu, Justin Crouse, and Douglas J. Gardner. The first draft of the manuscript was written by Xueqi Wang. Supervision, writing-reviewing, and editing were performed by Yucheng Peng, Shaoyang Liu, Brian Via, Thomas Elder, Tom Gallagher, and Douglas J. Gardner. All authors read and approved the manuscript.

ACKNOWLEDGMENTS

This work was supported by the Downed Timber Research program funded by USDA Forest Service Southern Research Station and the United States Endowment for Forestry and Communities. Additional support from the Alabama Agricultural Experiment Station and the Hatch program of the USDA National Institute of Food and Agriculture [ALA031-1-19091] was also appreciated. We also thank ExxonMobil Chemical Company for donating polypropylene for this research.

CONFLICT OF INTEREST STATEMENT

The authors declare no conflict of interest.

DATA AVAILABILITY STATEMENT

The data that supporting the findings of this study are available from the corresponding author upon reasonable request.

ORCID

Xueqi Wang https://orcid.org/0009-0003-5542-9031

REFERENCES

1. Hao W, Wang M, Zhou F, et al. A review on nanocellulose as a lightweight filler of polyolefin composites. *Carbohydr Polym*. 2020;243:116466. doi:10.1016/j.carbpol.2020.116466
2. Nagarajan K, Ramanujam N, Sanjay M, et al. A comprehensive review on cellulose nanocrystals and cellulose nanofibers: pretreatment, preparation, and characterization. *Polym Compos*. 2021;42(4):1588-1630. doi:10.1002/pc.25929
3. Ganapathy V, Muthukumaran G, Sudhagar PE, et al. Mechanical properties of cellulose-based multiscale composites: a review. *Polym Compos*. 2023;44(2):734-756. doi:10.1002/pc.27175
4. Dufresne A. Nanocellulose: potential reinforcement in composites. *Nat Polym*. 2012;2:1-32.
5. Moon RJ, Martini A, Nairn J, Simonsen J, Youngblood JJCSR. Cellulose nanomaterials review: structure, properties and nanocomposites. *Chem Soc Rev*. 2011;40(7):3941-3994. doi:10.1039/C0CS00108B
6. Sabo RC, Elhajjar RF, Clemons CM, Pillai KM. Characterization and processing of nanocellulose thermosetting composites. *Handbook of Polymer Nanocomposites Processing, Performance and Application*, Springer Berlin, Heidelberg; 2015:265-295.
7. Pandey J, Chu W, Kim C, Lee C, Ahn S. Bio-nano reinforcement of environmentally degradable polymer matrix by cellulose whiskers from grass. *Compos Part B: Eng*. 2009;40(7):676-680. doi:10.1016/j.compositesb.2009.04.013
8. Kargarzadeh H, Sheltami RM, Ahmad I, Abdullah I, Dufresne A. Cellulose nanocrystal: a promising toughening agent for unsaturated polyester nanocomposite. *Polymer*. 2015;56:346-357.
9. Khoshkava V, Kamal MR. Effect of cellulose nanocrystals (CNC) particle morphology on dispersion and rheological and mechanical properties of polypropylene/CNC nanocomposites. *ACS Appl Mater Interfaces*. 2014;6(11):8146-8157. doi:10.1021/am500577e
10. Kargarzadeh H, Mariano M, Huang J, et al. Recent developments on nanocellulose reinforced polymer nanocomposites: a review. *Polymer*. 2017;132:368-393. doi:10.1016/j.polymer.2017.09.043
11. Alloin F, D'aprea A, Dufresne A, Kissi NE, Bossard F. Poly (oxyethylene) and ramie whiskers based nanocomposites: influence of processing: extrusion and casting/evaporation. *Cellulose*. 2011;18:957-973.
12. Sun M, Zhang L, Li C. Modified cellulose nanocrystals based on SI-ATRP for enhancing interfacial compatibility and mechanical performance of biodegradable PLA/PBAT blend. *Polym Compos*. 2022;43(6):3753-3764. doi:10.1002/pc.26653
13. Mousavi SR, Faraj Nejad S, Jafari M, Paydayesh A. Polypropylene/ethylene propylene diene monomer/cellulose nanocrystal ternary blend nanocomposites: effects of different parameters on mechanical, rheological, and thermal properties. *Polym Compos*. 2021;42(9):4187-4198. doi:10.1002/pc.26137
14. Norrrahim MNF, Tengku Yasim-Anuar TA, Sapuan S, et al. Nanocellulose reinforced polypropylene and polyethylene composite for packaging application. SM Sapuan, RA Ilyas, CV Stevens, (eds). *Bio-Based Packaging: Material, Environmental Economic Aspects*, Wiley; 2021:133-150. doi:10.1002/9781119381228.ch8
15. Dem K. Polyethylene vs Polypropylene: When to Choose What? The material selection platform. Accessed May 24, 2023. https://omnexus.specialchem.com/tech-library/article/polyethylene-versus-polypropylene

16. Sojoudiasli H, Heuzey MC, Carreau PJ. Mechanical and morphological properties of cellulose nanocrystal-polypropylene composites. *Polym Compos*. 2018;39(10):3605-3617. doi:10.1002/pc.24383
17. Ljungberg N, Bonini C, Bortolussi F, Boisson C, Heux L, Cavaillé J-Y. New nanocomposite materials reinforced with cellulose whiskers in atactic polypropylene: effect of surface and dispersion characteristics. *Biomacromolecules*. 2005;6(5):2732-2739. doi:10.1021/bm050222v
18. Bahar E, Ucar N, Onen A, et al. Thermal and mechanical properties of polypropylene nanocomposite materials reinforced with cellulose nano whiskers. *J Appl Polym Sci*. 2012;125(4):2882-2889. doi:10.1002/app.36445
19. Khoshkava V, Kamal M. Effect of drying conditions on cellulose nanocrystal (CNC) agglomerate porosity and dispersibility in polymer nanocomposites. *Powder Technol*. 2014;261:288-298. doi:10.1016/j.powtec.2014.04.016
20. Peng Y, Gardner DJ, Han Y. Drying cellulose nanofibrils: in search of a suitable method. *Cellul*. 2012;19:91-102.
21. Wang Q, Yao Q, Liu J, Sun J, Zhu Q, Chen H. Processing nanocellulose to bulk materials: a review. *Cellulose*. 2019;26:7585-7617.
22. Alarcón-Moyano J, Acuña D, Matiacevich S, et al. Physico-chemical and structural characterization of cellulose nanocrystals obtained by two drying methods: freeze-drying and spray-drying. *Food Hydrocoll*. 2023;140:108571. doi:10.1016/j.foodhyd.2023.108571
23. Peng Y, Han Y, Gardner DJ. Spray-drying cellulose nanofibrils: effect of drying process parameters on particle morphology and size distribution. *Wood Fiber Sci*. 2012;44(4):448-461.
24. Tanpichai S, Oksman K. Cross-linked nanocomposite hydrogels based on cellulose nanocrystals and PVA: mechanical properties and creep recovery. *Compos Part A: Appl Sci Manuf*. 2016;88:226-233.
25. Xu X, Liu F, Jiang L, Zhu J, Haagenson D, Wiesenborn D. Cellulose nanocrystals vs. cellulose nanofibrils: a comparative study on their microstructures and effects as polymer reinforcing agents. *ACS Appl Mater Interfaces*. 2013;5(8):2999-3009.
26. DiLoreto E, Haque E, Berman A, Moon RJ, Kalaitzidou K. Freeze dried cellulose nanocrystal reinforced unsaturated polyester composites: challenges and potential. *Cellulose*. 2019;26:4391-4403.
27. Zhang X, Zhang Y. Reinforcement effect of poly (butylene succinate) (PBS)-grafted cellulose nanocrystal on toughened PBS/-polylactic acid blends. *Carbohydr Polym*. 2016;140:374-382. doi:10.1016/j.carbpol.2015.12.073
28. Agarwal J, Mohanty S, Nayak SK. Valorization of pineapple peel waste and sisal fiber: study of cellulose nanocrystals on polypropylene nanocomposites. *J Appl Polym Sci*. 2020;137(42):49291. doi:10.1002/app.49291
29. Kang H, Kim DS. A study on the crystallization and melting of PLA nanocomposites with cellulose nanocrystals by DSC. *Polym Compos*. 2023;1-10. doi:10.1002/pc.27658
30. Siqueira G, Bras J, Dufresne A. Cellulose whiskers versus microfibrils: influence of the nature of the nanoparticle and its surface functionalization on the thermal and mechanical properties of nanocomposites. *Biomacromolecules*. 2009;10(2):425-432. doi:10.1021/bm801193d
31. Khoshkava V, Ghasemi H, Kamal MR. Effect of cellulose nanocrystals (CNC) on isothermal crystallization kinetics of polypropylene. *Thermochim Acta*. 2015;608:30-39. doi:10.1016/j.tca.2015.04.007
32. Corrêa AC, Teodoro KBR, Simão JA, et al. Cellulose nanocrystals from curaua fibers and poly [ethylene-co-(vinyl acetate)] nanocomposites: effect of drying process of CNCs on thermal and mechanical properties. *Polym Compos*. 2020;41(5):1736-1748. doi:10.1002/pc.25493
33. Gray DG. Transcrystallization of polypropylene at cellulose nanocrystal surfaces. *Cellulose*. 2008;15:297-301.
34. Kamal MR, Khoshkava V. Effect of cellulose nanocrystals (CNC) on rheological and mechanical properties and crystallization behavior of PLA/CNC nanocomposites. *Carbohydr Polym*. 2015;123:105-114. doi:10.1016/j.carbpol.2015.01.012
35. Peng Y, Gallegos SA, Gardner DJ, Han Y, Cai Z. Maleic anhydride polypropylene modified cellulose nanofibril polypropylene nanocomposites with enhanced impact strength. *Polym Compos*. 2016;37(3):782-793. doi:10.1002/pc.23235
36. Wang L, Roach AW, Gardner DJ, Han Y. Mechanisms contributing to mechanical property changes in composites of polypropylene reinforced with spray-dried cellulose nanofibrils. *Cellulose*. 2018;25:439-448.
37. Bagheriasl D, Carreau P, Dubois C, Riedl B. Properties of polypropylene and polypropylene/poly (ethylene-co-vinyl alcohol) blend/CNC nanocomposites. *Compos Sci Technol*. 2015;117:357-363. doi:10.1016/j.compscitech.2015.07.012
38. Aumnate C, Rudolph N, Sarmadi M. Recycling of polypropylene/polyethylene blends: effect of chain structure on the crystallization behaviors. *Polymers*. 2019;11(9):1456. doi:10.3390/polym11091456
39. Voronova M, Surov O, Zakharov A. Nanocrystalline cellulose with various contents of sulfate groups. *Carbohydr Polym*. 2013;98(1):465-469. doi:10.1016/j.carbpol.2013.06.004
40. Brewis D, Briggs D. Adhesion to polyethylene and polypropylene. *Polymer*. 1981;22(1):7-16. doi:10.1016/0032-3861(81)90068-9
41. Shang W, Huang J, Luo H, Chang PR, Feng J, Xie G. Hydrophobic modification of cellulose nanocrystal via covalently grafting of castor oil. *Cellulose*. 2013;20(1):179-190.
42. Dufresne A. Nanocellulose: a new ageless bionanomaterial. *Mater Today*. 2013;16(6):220-227.
43. Peng Y, Musah M, Via B, Wang X. Calcium carbonate particles filled homopolymer polypropylene at different loading levels: mechanical properties characterization and materials failure analysis. *J Compos Sci*. 2021;5(11):302.
44. Zheng H, Zhang W, Li B, et al. Recent advances of interphases in carbon fiber-reinforced polymer composites: a review. *Compos Part B: Eng*. 2022;233:109639. doi:10.1016/j.compositesb.2022.109639
45. Garcia de Rodriguez NL, Thielemans W, Dufresne A. Sisal cellulose whiskers reinforced polyvinyl acetate nanocomposites. *Cellulose*. 2006;13(3):261-270.
46. Mathew AP, Gong G, Bjorngrim N, Wixe D, Oksman KS. Moisture absorption behavior and its impact on the mechanical properties of cellulose whiskers-based polyvinylacetate nanocomposites. *Polym Eng Sci*. 2011;51(11):2136-2142. doi:10.1002/pen.22063
47. Li VC-F, Kuang X, Mulyadi A, Hamel CM, Deng Y, Qi HJ. 3D printed cellulose nanocrystal composites through digital light processing. *Cellulose*. 2019;26(6):3973-3985.

48. Samarasekara A, Kumara S, Madhusanka A, Amarasinghe D, Karunanayake L. Study of thermal and mechanical properties of microcrystalline cellulose and nanocrystalline cellulose based thermoplastic material. IEEE; 2018:465-470.
49. Espert A, Vilaplana F, Karlsson S. Comparison of water absorption in natural cellulosic fibres from wood and one-year crops in polypropylene composites and its influence on their mechanical properties. *Compos Part A: Appl Sci Manuf*. 2004; 35(11):1267-1276. doi:10.1016/j.compositesa.2004.04.004
50. Ashori A, Sheshmani S. Hybrid composites made from recycled materials: moisture absorption and thickness swelling behavior. *Bioresour Technol*. 2010;101(12):4717-4720. doi:10.1016/j.biortech.2010.01.060
51. Amash A, Zugenmaier P. Morphology and properties of isotropic and oriented samples of cellulose fibre–polypropylene composites. *Polymer*. 2000;41(4):1589-1596. doi:10.1016/S0032-3861(99)00273-6
52. Agarwal J, Mohanty S, Nayak SK. Influence of cellulose nanocrystal/sisal fiber on the mechanical, thermal, and morphological performance of polypropylene hybrid composites. *Polym Bull*. 2021;78:1609-1635.
53. Shin H, Kim S, Kim J, Kong S, Lee Y, Lee JC. Preparation of 3-pentadecylphenol-modified cellulose nanocrystal and its application as a filler to polypropylene nanocomposites having improved antibacterial and mechanical properties. *J Appl Polym Sci*. 2022;139(13):51848. doi:10.1002/app.5184
54. Lamaming J, Hashim R, Sulaiman O, Leh CP, Sugimoto T, Nordin NA. Cellulose nanocrystals isolated from oil palm trunk. *Carbohydr Polym*. 2015;127:202-208. doi:10.1016/j.carbpol.2015.03.043
55. Roman M, Winter WT. Effect of sulfate groups from sulfuric acid hydrolysis on the thermal degradation behavior of bacterial cellulose. *Biomacromolecules*. 2004;5(5):1671-1677. doi:10.1021/bm034519+
56. Peng Y, Gardner DJ, Han Y, Kiziltas A, Cai Z, Tshabalala MA. Influence of drying method on the material properties of nanocellulose I: thermostability and crystallinity. *Cellulose*. 2013; 20(5):2379-2392.
57. Qiu W, Zhang F, Endo T, Hirotsu T. Preparation and characteristics of composites of high-crystalline cellulose with polypropylene: effects of maleated polypropylene and cellulose content. *J Appl Polym Sci*. 2003;87(2):337-345. doi:10.1002/app.11446
58. Kim D-Y, Nishiyama Y, Wada M, Kuga S. High-yield carbonization of cellulose by sulfuric acid impregnation. *Cellulose*. 2001;8(1):29-33.
59. Prado KS, Spinacé MA. Isolation and characterization of cellulose nanocrystals from pineapple crown waste and their potential uses. *Int J Biol Macromol*. 2019;122:410-416.
60. Yu Y, Fu S, Song P, et al. Functionalized lignin by grafting phosphorus-nitrogen improves the thermal stability and flame retardancy of polypropylene. *Polym Degrad Stab*. 2012;97(4):541-546. doi:10.1016/j.polymdegradstab.2012.01.020
61. Haq S, Srivastava R. Wood polypropylene (PP) composites manufactured by mango wood waste with virgin or recycled PP: mechanical, morphology, melt flow index and crystalline behaviour. *J Polym Environ*. 2017;25(3):640-648.
62. Jam NJ, Behravesh AH. Flow behavior of HDPE-fine wood particles composites. *J Thermoplast Compos Mater*. 2007;20(5): 439-451.
63. Kumari R, Ito H, Takatani M, Uchiyama M, Okamoto T. Fundamental studies on wood/cellulose-plastic composites: effects of composition and cellulose dimension on the properties of cellulose/PP composite. *J Wood Sci*. 2007;53(6):470-480.
64. Fonseca-Valero C, Ochoa-Mendoza A, Arranz-Andrés J, González-Sánchez C. Mechanical recycling and composition effects on the properties and structure of hardwood cellulose-reinforced high density polyethylene eco-composites. *Compos Part A: Appl Sci Manuf*. 2015;69:94-104.

How to cite this article: Wang X, Wang P, Liu S, et al. Material properties of spray-dried cellulose nanocrystal reinforced homopolymer polypropylene composites. *Polym Compos*. 2023; 1-15. doi:10.1002/pc.27806